Available online at www.sciencedirect.com
ScienceDirect
C. R. Chimie 11 (2008) 387–397
COMPTES RENDUS CHIMIE
http://france.elsevier.com/direct/CRAS2C/

Full paper / Mémoire

Efficiency of dipolar and *J*-derived solid-state NMR techniques for a new pair of nuclei $\{^{31}P,^{29}Si\}$. Towards the characterization of Si–O–P mesoporous materials

Cristina Coelho [a], Thierry Azais [a], Christian Bonhomme [a,*], Laure Bonhomme-Coury [a], Cédric Boissière [a], Guillaume Laurent [a], Dominique Massiot [b]

[a] *Laboratoire de chimie de la matière condensée de Paris, Université Pierre-et-Marie-Curie–Paris-6, UMR 7574, 4, place Jussieu, 75005 Paris, France*
[b] *CRMHT-CNRS, 1D, avenue de la Recherche-Scientifique, Orléans, France*

Received 27 April 2007; accepted after revision 28 September 2007
Available online 20 February 2008

Abstract

Solid-state NMR methods based on dipolar and *J*-derived experiments such as CP, MAS-*J*-HMQC and MAS-*J*-INEPT MAS have been developed in the frame of the $\{^{31}P,^{29}Si\}$ spin pair. The potential of these techniques has been demonstrated using model compounds including crystalline silicophosphate phases ($Si_5O(PO_4)_6$ and various SiP_2O_7 polymorphs). *Spatial* interactions as well as *through-bond* connectivities were established. Evaluation of isotropic $^2J_{P-O-Si}$ coupling constants has been established by careful analysis of the HMQC and INEPT build-up curves under fast MAS. The efficiency of the $^{31}P \rightarrow {}^{29}Si$ CP MAS experiment for the detailed characterization of Si–O–P mesoporous materials (at low temperature) was demonstrated. The incorporation of P atoms in the silica network has been proved unambiguously. Such materials could be appropriate for biocompatibility purposes. ***To cite this article: C. Coelho et al., C. R. Chimie 11 (2008).***

Résumé

Des méthodes de RMN en phase solide fondées sur l'interaction dipolaire (polarisation croisée en rotation à l'angle magique) et l'interaction de couplage *J* (MAS-*J*-HMQC et MAS-*J*-INEPT) ont été développées dans le cadre de la paire de spins $\{^{31}P,^{29}Si\}$. La mise au point de ces séquences a été effectuée à l'aide de composés modèles, comme $Si_5O(PO_4)_6$ et certains polymorphes de SiP_2O_7. Les *proximités spatiales* ainsi que les *connectivités chimiques* sont ainsi mises en évidence. L'évaluation des constantes isootropes de couplage $^2J_{P-O-Si}$ a été permise grâce à l'analyse détaillée des courbes d'évolution HMQC et INEPT. L'efficacité de la séquence $^{31}P \rightarrow {}^{29}Si$ CP MAS est démontrée dans le cadre de l'étude de matériaux mésoporeux de type Si–O–P. L'incorporation des atomes de phosphore au sein du réseau de silice est ainsi prouvée. Ces composés sont des candidats potentiels dans le cadre des matériaux biocompatibles. ***Pour citer cet article : C. Coelho et al., C. R. Chimie 11 (2008).***

* Corresponding author.
E-mail address: bonhomme@ccr.jussieu.fr (C. Bonhomme).

1631-0748/$ - see front matter © 2007 Académie des sciences. Published by Elsevier Masson SAS. All rights reserved.
doi:10.1016/j.crci.2007.09.012

Keywords: Silicophosphate; Solid-state NMR; Cross-polarization; *J* Coupling; Mesoporous materials

Mots-clés : Silicophosphate ; RMN en phase solide ; Polarisation croisée ; Couplage *J* ; Matériaux mésoporeux

1. Introduction

In the last few years, mesoporous materials attracted much attention due to their potential applications in several fields, including catalysis, polymerization, photochemistry…[1]. The silica-based MCM-41 structure is known to act as a bioactive material. Indeed, the intrinsic porosity of such material offers a wide range of possibilities for hosting molecules and the ability for drug delivery [2,3]. Recently, several researchers have been interested in the incorporation of bisphosphonates [4] in the pores of mesostructured silica, which may inhibit bone resorption. Confinement of such molecules could offer new opportunities such as bone reconstruction. The direct synthesis of Si–O–P mesoporous materials has been very rarely reported in the literature [5,6] and has received little attention.

In the field of materials, the local structure of nuclei can be probed efficiently by solid-state NMR spectroscopy. A large panel of techniques can be implemented for establishing *connectivities* between nuclei. It includes cross-polarization and *J*-derived experiments. The CP MAS (cross-polarization magic-angle spinning) sequence [7] relies on *dipolar* interaction. Such experiment establishes *spatial* proximities between X and Y nuclei. For X = ^{31}P and Y = ^{29}Si, very few results have been reported so far in the literature. These results are related to silicon phosphide (involving direct ^{31}P–^{29}Si bonds) [8] and silicophosphates involving ^{31}P–O–^{29}Si groups [9]. *J*-derived experiments based on the isotopic scalar *J* coupling constants establish X–Y *through-bond* connectivities. In the early 1990s, such solid-state NMR sequences were implemented successfully by Fyfe et al. [10] and Eckert et al. [11]. More recently, several groups showed that a large number of *J* experiments could be easily transposed to solid-state NMR. Among these, we find the HMQC (heteronuclear multiple quantum coherence) sequence, which has been adapted for the following spin pairs: ^{1}H/^{13}C, ^{1}H/^{15}N, ^{31}P/^{27}Al, ^{27}Al/^{17}O, ^{31}P/^{29}Si and ^{31}P/^{71}Ga [11–17]. The INEPT (insensitive nuclei enhanced by polarization transfer) sequence [18] is one of the most important pulse blocks in modern solution state experiments [19]. In solid-state NMR, the INEPT sequence was adapted for the study of mobile [20] and rigid [21] organic and hybrid systems. Examples related to inorganic components have been rarely reported in the literature [22–26].

In this paper, the complete study of silicophosphate phases such as $Si_5O(PO_4)_6$ and various SiP_2O_7 polymorphs is presented. The efficiency of ^{31}P → ^{29}Si CP MAS, MAS-*J*-HMQC and MAS-*J*-INEPT experiments involving the {^{31}P,^{29}Si} spin pair is demonstrated. The ^{31}P → ^{29}Si CP MAS experiment has been then successfully applied for the structural characterization of Si–O–P derived mesoporous materials. Such materials were obtained via an aerosol process. The incorporation of phosphorus in the silica network at atomic level was clearly demonstrated.

2. Experimental: syntheses and solid-state NMR

Solid-state NMR experiments were performed on a Bruker Avance 300 spectrometer at $B_0 = 7$ T with ν_0 (^{31}P) = 121.49 MHz and ν_0 (^{29}Si) = 59.63 MHz, using a 4-mm triple resonance Bruker MAS probe. Samples were spun at the magic angle using ZrO_2 rotors (5–14 kHz). ^{31}P chemical shifts were referenced to 85% aqueous H_3PO_4. ^{29}Si chemical shifts were referenced to TMS. In the case of mesoporous materials, all experiments were obtained at low temperature ($T = 238$ K), thanks to a cooling unit (BCU-X), a control temperature unit, and a DVT probe. The calibration of the temperature was performed using lead nitrate, $Pb(NO_3)_2$. Full experimental details are given in the figure captions. The X-ray diffraction patterns of mesoporous materials were obtained using a D8 Advance Bruker diffractometer (Cu Kα radiation: $\lambda = 1.54718$ Å, 1–6° in 2θ with a step size of 0.02° in 2θ, scan rate: 5 s/step). For TEM experiments (Philips Technai 12), samples were dispersed in ethanol and dropped onto a copper grid covered with carbon.

The synthesis protocols are the following: *$Si_5O(PO_4)_6$*: TEOS ($Si(OCH_2CH_3)_4$), ethanol and distilled water were used as precursors (TEOS/EtOH/H_2O = 1:4:3). The phosphorus precursor H_3PO_4 (85%) was added (Si/P = 1:1) at room temperature. The reaction was slightly exothermic. The addition of 1% (molar ratio) of a paramagnetic complex ($NiCl_2 \cdot 6H_2O$) was performed for NMR relaxation purposes, leading to a slightly green solution. After stirring at 25 °C, a transparent green wet gel was obtained (2 h). The final powder was

obtained after heat treatment at 800 °C for 2 h. The structure of $Si_5O(PO_4)_6$ described by Mayer [27] (trigonal, $R\bar{3}$, $a = 7.869$ Å, $c = 24.138$ Å, JCPDS: 70-2071) involves one unique P site and three inequivalent Si sites (two 6-fold coordinated atoms Si_{VI}, Si(1) and Si(2), and one 4-fold coordinated atom Si_{IV}, Si(3)). The Si(1)/Si(2)/Si(3) ratio is 1:2:2. The structure consists of $[SiO_6]$ and $[Si_2O_7]$ groups linked by $[PO_4]$ groups. Each $[PO_4]$ tetrahedron is surrounded by three Si_{VI} atoms (Si(2) (×2) and Si(1)) and one Si_{IV} atom (Si(3)) (Fig. 1). Si(1) is bonded to six equivalent oxygen atoms O(3) (Si(1)–O(3) = 1.756 Å, Si(1)O(3)P = 145.58°). Si(2) is bonded to six oxygen atoms, but two inequivalent oxygen atoms (O(2) and O(5)) are involved ((2) = 1.791 Å, Si(2)–O(5) = 1.756 Å, Si(2)O(2)P = 131.15°, Si(2)O(5)P = 151.38°). Si(3) is bonded to four oxygen atoms, namely O(4) (×3) and O(1) (Si(3)–O(4) = 1.611 Å, Si(3)O(4)P = 138.83°, Si(3)–O(1) = 1.593 Å, Si(3)O(1)Si(3) = 180°). The ^{31}P MAS NMR spectrum reveals a unique resonance located at δ (^{31}P) = −43.8 ppm, while the ^{29}Si MAS NMR spectrum exhibits three resonances located at δ (^{29}Si) = −119.3, −213.5, and −217.3 ppm (Fig. 1 and Table 1). A broad resonance located at δ (^{29}Si) ∼ −113 ppm associated with amorphous silica (side product) is also evidenced.

2.1. Mixture of SiP_2O_7 polymorphs and $Si_5O(PO_4)_6$

After the dissolution of $NiCl_2 \cdot 6H_2O$ (1%) in ethanol, H_3PO_4 (85%) was added, followed by TEOS (Si/P = 1:2). A gel was obtained after 2 h at room temperature, heated at 100 °C for 48 h, and further heat-treated at 1000 °C for 2 h. The X-ray diffraction (XRD) powder pattern of the sample (not shown here) indicates that besides the $Si_5O(PO_4)_6$ crystalline phase

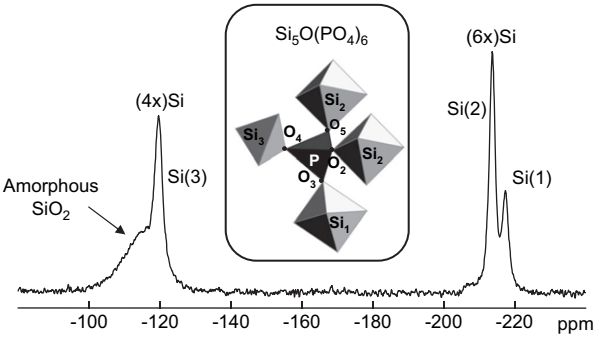

Fig. 1. Part of the structure of $Si_5O(PO_4)_6$ around the unique P atom. The labelling scheme of atoms is given according to Ref. [27]. ^{29}Si MAS spectrum (single pulse experiment) (∅ = 4 mm, rotation frequency (RO) = 14 kHz, number of scans (NS) = 1760, recycle delay (RD) = 10 s, 90° (^{29}Si) = 4.5 μs, LB = 10 Hz).

Table 1
^{31}P and ^{29}Si isotropic chemical shifts for the mixture of $Si_5O(PO_4)_6$ and SiP_2O_7 polymorphs [15]

Phase (JCPDS)	δ_{iso} (ppm)	
	^{29}Si (Fig. 1)	^{31}P (Fig. 2)
$Si_5O(PO_4)_6$ (70-2071)	−119.3	−43.8
	−213.5	
	−217.3	
SiP_2O_7 tetragonal (22-1320)		−45.5
		−52.8
SiP_2O_7 monoclinic 1 (39-0189)		−47.6
		−55.3
SiP_2O_7 monoclinic 2 (25-0755)		−46.1
		−49.4
SiP_2O_7 cubic (22-1321)		∼−50
		∼−58
		∼−70

presented above, three polymorphs of SiP_2O_7 were synthesized as major constituents, namely a tetragonal (JCPDS: 22-1320) [28] and two monoclinic forms (JCPDS: 39-0189 and 25-0755) [29,30]. As shown in Fig. 2, the ^{31}P MAS NMR spectrum reveals also the presence of the SiP_2O_7 cubic form (JCPDS: 22-1321), but as a very minor component. This particular phase was not clearly evidenced by XRD. For the SiP_2O_7 polymorphs, it is known from XRD data that the pyrophosphate groups (involving generally two non-equivalent P sites) are linked exclusively to Si_{VI} atoms (Fig. 2). The ^{31}P and ^{29}Si isotropic chemical shifts of the various SiP_2O_7 polymorphs are reported in Table 1.

2.2. $SiP_{0.1}$-aerosol mesoporous derivative

At room temperature, 5 g (13.7 mmol) of the surfactant (CTAB, $C_{16}H_{33}N^+(CH_3)_3Br^-$) were dissolved in a solution of distilled water/ethanol. Then, 0.8 ml (11.6 mmol) of H_3PO_4 (85%) was added. The pH was then adjusted to 2.1 with HCl (2 M) before the addition of 23 ml of TEOS. The molar ratio was CTAB/TEOS/H_3PO_4: 0.14:1.0:0.10. The solution was then treated using the aerosol process. Some works have been already dedicated to the synthesis of mesoporous spheres obtained by this method [31]. The nanoparticles were produced in a reactor consisting of a spraying chamber combined with a tubular furnace and a filter. The final powder was heated at 310 °C and 500 °C in air to remove efficiently the surfactant and to obtain the final mesoporous silicophosphate materials.

3. Results and discussion

The various pulse schemes used in this work will be first presented. The full characterization of $Si_5O(PO_4)_6$

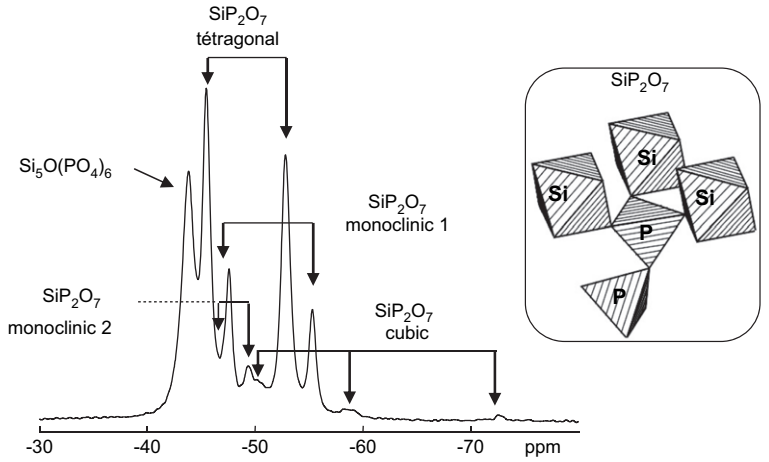

Fig. 2. Structural scheme for SiP_2O_7 pyrophosphate phases: one given P atom is bonded to one P atom and three equivalent 6-fold coordinated Si atoms. ^{31}P MAS spectrum of the mixture of $Si_5O(PO_4)_6$ and several polymorphs of SiP_2O_7 (tetragonal, monoclinic 1, monoclinic 2, and cubic) ($\varnothing = 4$ mm, RO = 14 kHz, NS = 8, RD = 5 s, 90° (^{31}P) = 6 μs, LB = 0 Hz).

and SiP_2O_7 polymorphs by CP MAS, MAS-*J*-HMQC and MAS-*J*-INEPT experiments are first shown, followed by the structural characterization of Si–O–P mesoporous materials.

3.1. Solid-state NMR methodology

3.1.1. $^{31}P \rightarrow {}^{29}Si$ HETCOR CP MAS experiment

The $^{31}P \rightarrow {}^{29}Si$ 2D HETCOR sequence presented in Fig. 3a is an extension of the 1D $^{31}P \rightarrow {}^{29}Si$ CP MAS experiment. For the set-up, the MAS rotation frequency was fixed at 5 kHz. Even at this moderate MAS rate, the Hartmann–Hahn (H–H) profile must split into sharp spinning sidebands (because of the small heteronuclear dipolar interaction involving ^{31}P and ^{29}Si). A VACP profile (variable amplitude cross-polarization) [32] was used during the contact time (t_{CP}), in order to broaden the H–H profile. The ^{29}Si acquisition was obtained under ^{31}P CW decoupling. A saturation loop (characterized by Δ and n) was applied on the ^{31}P channel before the first 90° pulse.

3.1.2. ^{31}P–^{29}Si MAS-J-HMQC experiment

The 2D ^{31}P–^{29}Si MAS-*J*-HMQC sequence is presented in Fig. 4a. T_2' time constants [15] were measured by spin-echo experiments (90°–τ'–180°–τ') under fast MAS for the unique ^{31}P signal. Such time constants are characteristic of the lifetime of the involved coherences. The experimental curve was fitted by a single exponential decay in time domain according to:

$$I = I_0 \exp\left(-2\tau'/T_2'\right) \qquad (1)$$

leading to T_2' (^{31}P) = 65 ± 3 ms. This long T_2' value is favourable to the creation and evolution of coherences during the HMQC pulse scheme. As the optimum τ value (Fig. 4a) for a given compound depends strongly on $^2J_{P-O-Si}$ values and T_2', various 1D ^{31}P–^{29}Si MAS-*J*-HMQC experiments at variable τ were performed (not presented here). For one given spin pair, the evolution of the HMQC signal as a function of τ can be modelled by [12a,33]:

$$I_{HMQC} = I_0 \sin^2(\pi J_{P-O-Si}\tau)\exp\left(-2\tau/T_2'\left(^{31}P\right)\right) \qquad (2)$$

Using Eq. (2) and taking into account a unique ^{31}P–^{29}Si coupling constant and T_2' (^{31}P) = 65 ms, an averaged $^2J_{P-O-Si}$ value could be extracted from the build-up data. This crude approach led to $^2J_{P-O-Si} \sim 15$ Hz [15].

3.1.3. ^{31}P–^{29}Si MAS-J-INEPT experiment

The pulse sequence for refocused 2D ^{31}P–^{29}Si MAS-*J*-INEPT experiment is shown in Fig. 5a. The original solution state technique [18] was adapted here for rotating solids and for a new pair of nuclei {^{31}P,^{29}Si}. Fast magic-angle spinning (usually 14 kHz) averages the chemical shift anisotropy and the heteronuclear dipolar couplings to zero, leaving only the scalar couplings and the isotropic chemical shifts [21]. The refocused INEPT pulse sequence consists of the following steps: a 90° pulse is applied to the ^{31}P channel, followed by an evolution delay optimized to achieve ^{31}P anti-phase magnetization. The refocusing of the isotropic chemical shifts is obtained by the simultaneous

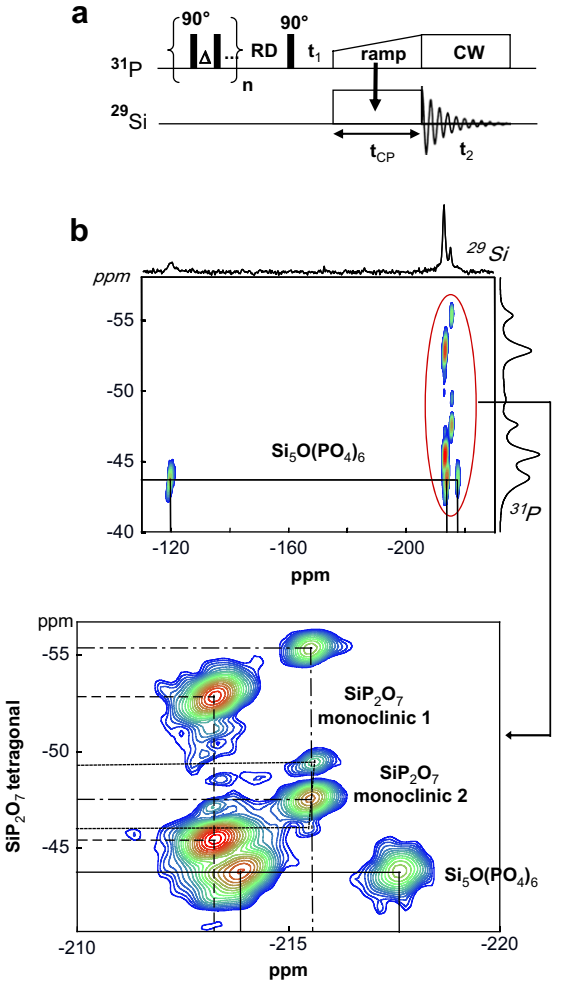

Fig. 3. (a) Pulse sequence for the 2D $^{31}P \rightarrow {}^{29}Si$ CP MAS HETCOR experiment. (b) 2D $^{31}P \rightarrow {}^{29}Si$ HETCOR CP MAS spectrum of the mixture of $Si_5O(PO_4)_6$ and several polymorphs of SiP_2O_7 (∅: 4 mm, RO = 5 kHz, NS = 104 for each t_1 increment, RD = 10 s, 90° (^{31}P) = 5.3 μs, t_{CP} = 40 ms, State mode with 384 t_1 increments, LB = 10 Hz in F2 (^{29}Si), LB = 20 Hz in F1 (^{31}P)). The zoomed region corresponds to the 6-fold coordinated ^{29}Si nuclei.

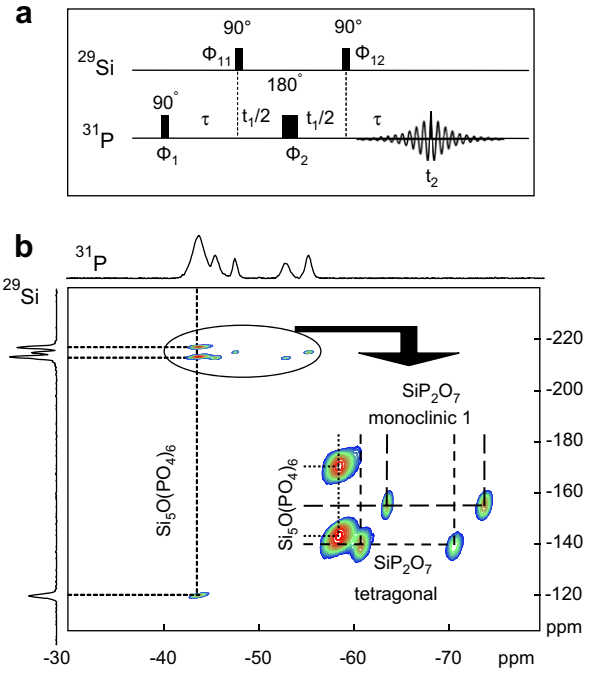

Fig. 4. (a) 2D $^{31}P-{}^{29}Si$ MAS-*J*-HMQC pulse sequence. $\Phi_1 = +x$; $\Phi_2 = +x, +x, +y, +y, -x, -x, -y, -y$; $\Phi_{11} = +x$; $\Phi_{12} = +x, -x$; receiver = $+x, -x, -x, +x, +x, -x, -x, +x$. (b) $^{31}P-{}^{29}Si$ 2D MAS-*J*-HMQC spectrum of the mixture of $Si_5O(PO_4)_6$ and SiP_2O_7 polymorphs (∅ = 4 mm, RO = 14 kHz, NS = 136 for each t_1 increment, RD = 5 s, 90° (^{31}P) = 6.8 μs, 90° (^{29}Si) = 5.3 μs, τ = 25 ms, State mode with 208 t_1 increments, LB = 0 Hz in F2 (^{31}P), LB = 0 Hz in F1 (^{29}Si), presaturation on the ^{31}P channel). Below: expansion of the oval region.

application of 180° pulses on both phosphorus-31 and silicon-29 channels (only the $^2J_{P-O-Si}$ couplings have to be taken into account). For a pair of ^{31}P and ^{29}Si nuclei involved in a $^{31}P-O-{}^{29}Si$ group, anti-phase phosphorus-31 coherence with respect to silicon-29 is created after the first $\tau-\pi-\tau$ period. The two simultaneous 90° pulses lead to anti-phase silicon-29 coherence. The refocusing period $\tau'-\pi-\tau'$ is then applied to obtain in-phase ^{29}Si magnetization. ^{31}P decoupling is finally applied during the acquisition of the ^{29}Si signal.

In the MAS-*J*-INEPT experiment, τ and τ' delays must be carefully optimized. Such parameters involve not only the value of the $^2J_{P-O-Si}$ coupling constants, but also the relaxation time T_2' associated with each site. Table 2 presents an estimation of the T_2' (^{29}Si) and T_2' (^{31}P) values. For the refocused INEPT experiment, and considering a *unique* $^2J_{P-O-Si}$ coupling constant, the signal intensity is given by [19,34]:

$$I_{INEPT}(\tau,\tau') = I_0 \sin(2\pi J_{P-O-Si}\tau)\sin(2\pi J_{P-O-Si}\tau') \times \cos^{n-1}(2\pi J_{P-O-Si}\tau')\exp\left(-2\tau/T_2'(^{31}P)\right) \times \exp\left(-2\tau'/T_2'(^{29}Si)\right) \quad (3)$$

where n is the bond multiplicity (i.e., SI_n spin system with S ≡ ^{29}Si and I ≡ ^{31}P). An optimized τ delay of 11.4 ms will be used as a constant thereafter.

3.1.4. Results

Figs. 3b, 4b and 5b present the 2D $^{31}P-{}^{29}Si$ CP MAS HECTOR (with t_{CP} = 40 ms), 2D $^{29}Si-{}^{31}P$ MAS-*J*-HMQC (τ = 25 ms) and 2D $^{31}P-{}^{29}Si$ MAS-*J*-INEPT (τ = 11.4 ms and τ' = 4.6 ms) spectra of the $Si_5O(PO_4)_6SiP_2O_7$ mixture, respectively (see the

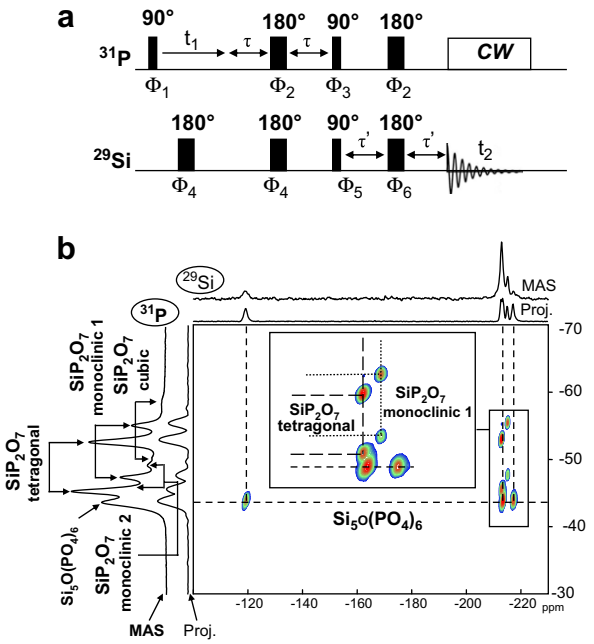

Fig. 5. (a) ^{31}P–^{29}Si 2D refocused MAS-*J*-INEPT pulse sequence. $\Phi_1 = +x, +x, +x, +x, +x, +x, +x, +x, -x, -x, -x, -x, -x, -x, -x, -x$; $\Phi_2 = +x, -x$; $\Phi_3 = +y, +y, -y, -y$; $\Phi_4 = +x, -x$; $\Phi_5 = +x, +x, +x, +x, +y, +y, +y, +y, -x, -x, -x, -x, -y, -y, -y, -y$; $\Phi_6 = +x, -x, +x, -x, +y, -y, +y, -y$; receiver $= +x, +x, -x, -x, +y, +y, -y, -y$. (b) 2D ^{31}P–^{29}Si refocused MAS-*J*-INEPT spectrum of the mixture of $Si_5O(PO_4)_6$ and SiP_2O_7 polymorphs ($\varnothing = 4$ mm, RO = 14 kHz, NS = 496 for each t_1 increment, RD = 5 s, 90° (^{29}Si) = 5.7 μs, 90° (^{31}P) = 4.3 μs, τ = 11.4 ms, $\tau' = 4.6$ ms, State mode with 128 t_1 increments, LB = 20 Hz in F2 (^{29}Si), LB = 20 Hz in F1 (^{31}P)). The expansion of the boxed region is presented in the figure. The projections of the 2D spectrum are also given.

synthesis above). Three cross-peaks associated $Si_5O(PO_4)_6$ phase are systematically observed (the unique ^{31}P site at −43.8 ppm is *J* and D coupled to the three ^{29}Si resonances − Fig. 1). Moreover, the 2D spectra reveal the presence of numerous cross-peaks (shown in the expansions in Figs. 3b, 4b and 5b), located in the *6-fold coordinated* ^{29}Si chemical shift range (∼−215 ppm). These cross-peaks are safely assigned to SiP_2O_7 polymorphs. Therefore, D and *J* 2D experiments are suitable to edit the ^{31}P MAS spectra in terms of pairs involved in each SiP_2O_7 pyrophosphate phase (Fig. 2). Moreover, the unique ^{29}Si isotropic shift corresponding to each SiP_2O_7 polymorph is determined with great accuracy. All ^{31}P and ^{29}Si isotropic chemical shifts are reported in Tables 3 and 4 (HECTOR and HMQC/INEPT experiments, respectively). Comparing the three experiments, we note that in the 2D ^{29}Si–^{31}P MAS-*J*-HMQC and MAS-*J*-INEPT spectra, no cross-peaks corresponding to the *monoclinic 2* form of SiP_2O_7 are observed. Such cross-peaks are observed in the case of the 2D HETCOR experiment (Fig. 3b). It is assumed that the *J* coupling constants are markedly different for the various SiP_2O_7 phases, leading to the underestimation of the monoclinic 2 form in *J*-derived experiments. The absence of observable cross-peaks for the cubic forms in the three experiments is due to the low amount of this particular phase (Fig. 2).

$Si_5O(PO_4)_6$ acted also as a model compound for the measurement of individual $^2J_{P-O-Si}$ coupling constants via the MAS-*J*-INEPT experiment. The INEPT build-up curves obtained vs τ' (at fixed $\tau = 11.4$ ms) for Si(1), Si(2) and Si(3) are presented in Fig. 6a, b and c, respectively. The variation of the intensity is clearly dependent on both the number of P atoms bonded to the silicon atoms ($n = 6$ for Si(1), Si(2); $n = 3$ for Si(3)) *and* the crystallographic characteristics of the various sites (for Si(1) and Si(2)). Eq. (3), as well as the T_2' constants presented in Table 2, were used for the fitting of the experimental curves for Si(1) and Si(3) (with $n = 6$ and $n = 3$, respectively). For both Si sites, a unique $^2J_{P-O-Si}$ coupling constant is involved. The extracted *J* value corresponds to $^2J_{P-O-Si} \approx 15$ and 12 Hz for Si(1) and Si(3), respectively [26]. Obviously, the Si(2) build-up curve differs drastically from the one obtained for Si(1), even though Si(1) and

Table 2
Estimated T_2' (^{29}Si) and T_2' (^{31}P) obtained using MAS spin echo experiments and Eq. (1) for the $Si_5O(PO_4)_6$ phase (Si(1), Si(2), Si(3) and P sites)

	T_2' (^{29}Si) (ms) [26]	T_2' (^{31}P) (ms) [15]
Si(1)–O–P	41 ± 4	65 ± 3
Si(2)–O–P	55 ± 4	
Si(3)–O–P	63 ± 5	

Table 3
^{31}P and ^{29}Si isotropic chemical shifts corresponding to the projections in the 2D ^{31}P–^{29}Si CP MAS HETCOR experiment for the mixture of $Si_5O(PO_4)_6$ and SiP_2O_7 polymorphs

Phase (JCPDS)	δ_{iso} (ppm)	
	^{31}P HETCOR (Fig. 3b)	^{29}Si HETCOR (Fig. 3b)
$Si_5O(PO_4)_6$ (70-2071)	−43.8	−119.6
		−213.8
		−217.6
SiP_2O_7 tetragonal (22-1320)	−45.4	−213.2
	−52.9	
SiP_2O_7 monoclinic 1 (39-0189)	−47.6	−215.5
	−55.4	
SiP_2O_7 monoclinic 2 (25-0755)	−46.0	−215.4
	−49.4	−215.6

Table 4
^{31}P and ^{29}Si isotropic chemical shifts corresponding to the projections in the 2D ^{31}P–^{29}Si MAS-*J*-HMQC and ^{31}P–^{29}Si MAS-*J*-INEPT experiments for the $Si_5O(PO_4)_6/SiP_2O_7$ polymorph mixture

Phase (JCPDS)	δ_{iso} (ppm)			
	^{31}P HMQC (Fig. 4b) [15]	^{29}Si HMQC (Fig. 4b) [15]	^{31}P INEPT (Fig. 5b) [26]	^{29}Si INEPT (Fig. 5b) [26]
$Si_5O(PO_4)_6$ (70-2071)	−43.8	−119.1	−43.9	−119.3
		−213.3		−213.5
		−217.0		−217.3
SiP_2O_7 tetragonal (22-1320)	−45.5	−212.8	−45.6	−213.0
	−52.9		−52.9	
SiP_2O_7 monoclinic 1 (39-0189)	−47.6	−214.9	−47.7	−215.3
	−55.3		−55.4	

Si(2) correspond both to 6-fold coordinated silicon atoms. In the case of Si(2), two different $^2J_{P-O-Si}$ coupling constants have to be a priori considered corresponding to Si(2)–O(2)–P and Si(2)–O(5)–P bonding paths (Fig. 6b). Considering two distinct *J* coupling constants (J_1 and J_2, $SI_3I'_3$ spin system), the product operator formalism [19] leads to:

$$I_{INEPT}(\tau,\tau') = I_0\cos^2(2\pi J_1\tau')\cos^2(2\pi J_2\tau')[\sin(2\pi J_1\tau)\sin(2\pi J_1\tau')\cos(2\pi J_2\tau') + \sin(2\pi J_2\tau)\sin(2\pi J_2\tau')\cos(2\pi J_1\tau')] \times \exp\left(-2\tau/T_2'(^{31}P)\right)\exp\left(-2\tau'/T_2'(^{29}Si)\right) \quad (4)$$

The fitting of Si(2) curve (Fig. 6b) leads to $J_1 \approx 14$ Hz and $J_2 \approx 4$ Hz [26]. The obtained J_2 value appears small, but we note that two distinct bond angles are involved in the case of Si(2): Si(2)–O(2)–P ≈ 131° and Si(2)–O(5)–P ≈ 151°. This is assumed to explain the strong difference between J_1 and J_2.

MAS-*J*-HMQC, MAS-*J*-INEPT and HETCOR CP MAS experiments are comparable in terms of experimental time. However, it must be noted that very long contact times (up to 40 ms) have to be used for efficient CP transfer (the ^{31}P/^{29}Si dipolar coupling is estimated to be ∼340 Hz in Si–O–P groups). The HMQC and INEPT sequences are obviously less demanding in terms of RF power, as short pulses are involved. Nevertheless, care must be taken when choosing the evolution periods, as T_2' relaxation processes have to be taken into account.

3.2. Mesoporous Si–O–P materials

Fig. 7a shows the X-ray diffraction pattern of the $SiP_{0.1}$-aerosol sample (see Section 2). The two observed peaks can be indexed as (100) and (110) reflections of a 2D hexagonal mesostructure. The TEM image of the powder presented in Fig. 7b shows the spherical morphology of the obtained nanoparticles (with diameters ranging from ∼50 to 300 nm).

^{1}H → X CP MAS experiments performed *at room temperature* showed systematically poor efficiency of polarization transfer. It is assumed that proton mobility strongly reduces the efficiency of the CP process. CP efficiency was indeed regained at low temperature ($T = 238$ K). The following spectra were recorded at $T = 238$ K. The ^{31}P MAS spectrum of the $SiP_{0.1}$-aerosol sample is shown in Fig. 7c. Four resonances at ∼2.5, −9.5, −23.0 and −38.3 ppm are evidenced, which can be assigned to Q'_N species, *N* ranging from 0 to 3 (see Table 5 for the definition of Q'_N and for the assignments). Protonated phosphate groups are evidenced by ^{1}H→ ^{31}P CP MAS experiment at $t_{CP} = 2$ ms (Fig. 7d). At this contact time, the resonance at ∼2.5 ppm corresponding to the Q'_0 specie is underestimated due to fast molecular motion even at low temperature. The other three resonances are assigned safely to protonated species, in agreement with notations presented in the literature [35]. The ^{29}Si MAS spectrum is presented in Fig. 7e. Two broad resonances at δ ∼−103 and ∼−111 ppm correspond to Q_3 and Q_4 species (Table 5). The corresponding ^{1}H → ^{29}Si CP MAS experiment is presented in Fig. 7f. Q3 units are overestimated, as it is usually the case in the case of silica gels and derivatives. Moreover, a weak amount of Q_2 units is evidenced: the corresponding resonance

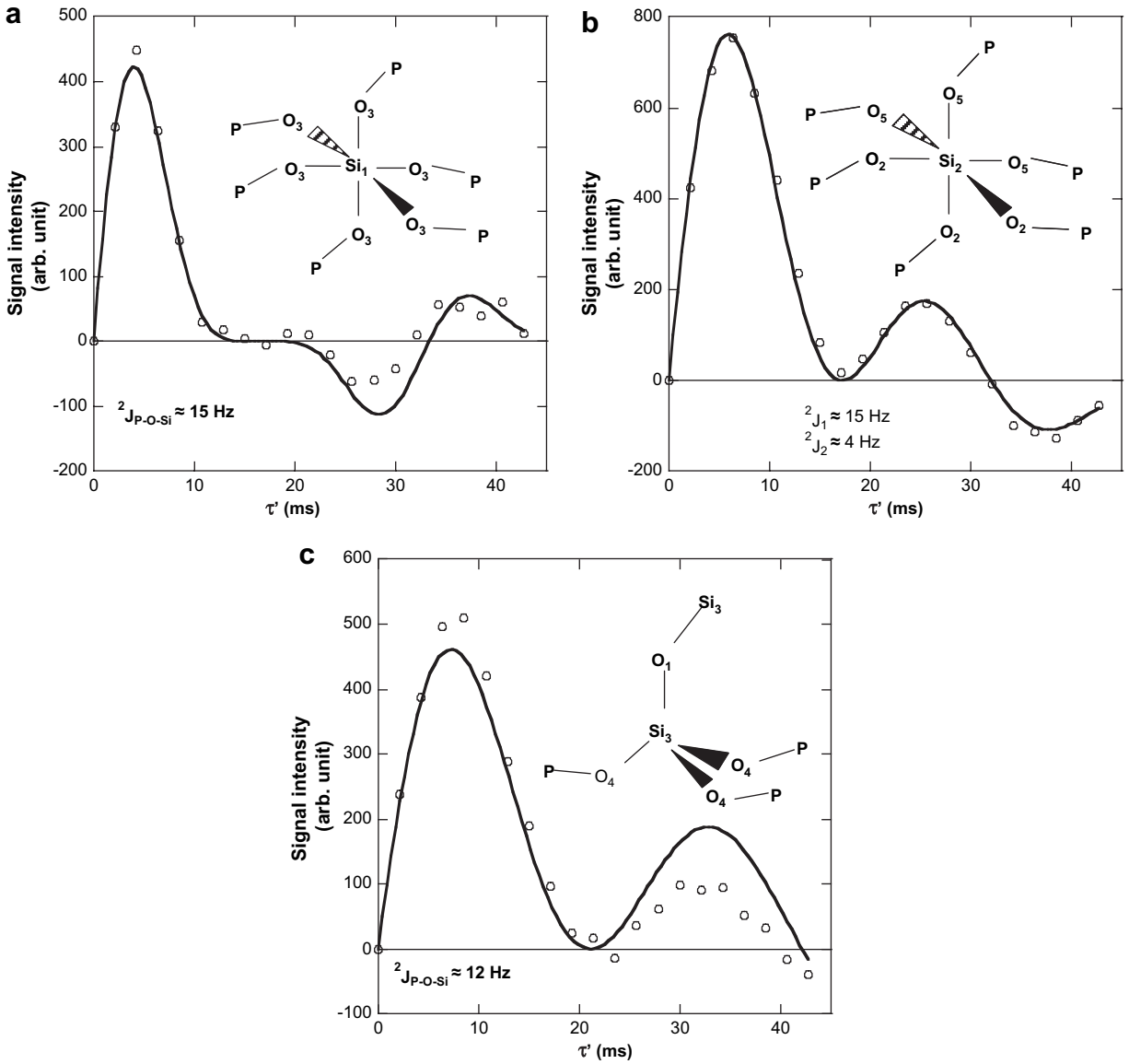

Fig. 6. (a–c) Experimental evolution of the $^{31}P-^{29}Si$ MAS-*J*-INEPT intensities as function of τ' (with fixed $\tau = 11.4$ ms) for Si(1), Si(2) and Si(3) ($Si_5O(PO_4)_6$ phase), respectively. The experimental data (o) were fitted by Eq. (3) for Si(1) and Si(3) and Eq. (4) for Si(2). The fixed T_2' constants are extracted from spin echo experiments (Table 2) ($\varnothing = 4$ mm, RO = 14 kHz, NS = 656, RD = 5 s, 90° (^{31}P) = 5 μs, 90° (^{29}Si) = 5.3 μs). Each Si site is depicted schematically.

is located at ∼−91 ppm. It has to be noticed that the notations used in Table 4 are rather loose. Indeed, various combinations of $^{29}Si-O-Si/^{29}Si-OH/^{29}Si-O-P$ bonds can lead to the same isotropic chemical shift value. Therefore, $^{31}P-^{29}Si$ CP MAS experiments appear as a valuable tool of investigation for the characterization of dipolar couplings within the mesoporous structure. The corresponding spectrum of the aerosol sample is presented in Fig. 7g. The signal-to-noise ratio is rather low due to the low amount of phosphorus used in the synthesis. Nevertheless, two resonances located at $\delta \sim -101$ (hardly discernable) and ∼−113 ppm can be detected. Such observations indicate the presence of Si···P dipolar contacts. These preliminary results are encouraging for an in-depth characterization of the structure of the Si–O–P mesoporous materials. $^1H \rightarrow {}^{29}Si \rightarrow {}^{31}P$ CP MAS experiments, as well as *J* experiments, should permit complete editing and assignment of both ^{31}P and ^{29}Si resonances in such materials.

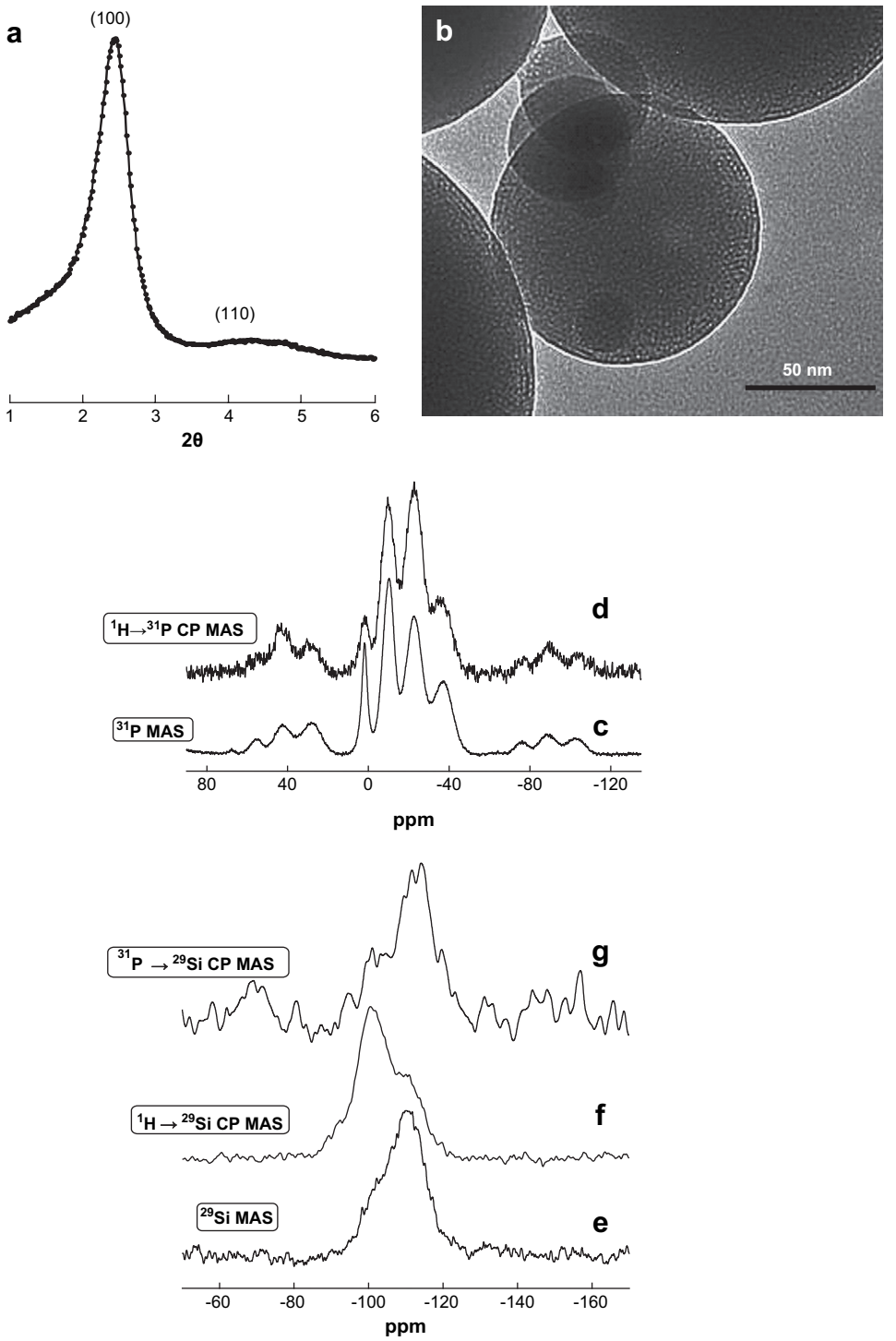

Fig. 7. (a) X-ray diffraction pattern (at low angle) of the $SiP_{0.1}$-aerosol sample. (b) TEM picture of the $SiP_{0.1}$-aerosol sample. (c) ^{31}P MAS NMR spectrum of $SiP_{0.1}$-aerosol sample at $T = 238$ K ($\varnothing = 4$ mm, RO = 8 kHz, NS = 1080, RD = 20 s, 90° (^{31}P) = 3.9 μs, TPPM 15 decoupling). (d) ^{1}H → ^{31}P CP MAS spectrum of $SiP_{0.1}$-aerosol sample at $T = 238$ K ($\varnothing = 4$ mm, RO = 8 kHz, NS = 112, RD = 2 s, 90° (^{1}H) = 5.3 μs, $t_{CP} = 2$ ms, TPPM 15 decoupling, LB = 20 Hz). (e) ^{29}Si MAS spectrum of $SiP_{0.1}$-aerosol sample at $T = 238$ K ($\varnothing = 4$ mm, RO = 8 kHz, NS = 184, RD = 60 s, 90° (^{29}Si) = 5.1 μs, TPPM decoupling, LB = 30 Hz). (f) ^{1}H → ^{29}Si CP MAS spectrum of $SiP_{0.1}$-aerosol sample at $T = 238$ K ($\varnothing = 4$ mm, RO = 8 kHz, NS = 2040, RD = 3 s, 90° (^{1}H) = 5.3 μs, $t_{CP} = 10$ ms, TPPM 15 decoupling, LB = 50 Hz). (g) ^{31}P → ^{29}Si CP MAS spectrum of $SiP_{0.1}$-aerosol sample at $T = 238$ K ($\varnothing = 4$ mm, RO = 8 kHz, NS = 22456, RD = 10 s, 90° (^{31}P) = 5.1 μs, $t_{CP} = 10$ ms, CW {^{31}P} decoupling, LB = 100 Hz, presaturation on the ^{31}P).

Table 5
Proposed assignments for ^{31}P and ^{29}Si isotropic resonances

δ (ppm)	Assignment
(^{31}P)	
~0	O=P(OH)$_3$
−10/−20	O=P(OH)$_2$(OP/OSi)
−20/−25	O=P(OH)(OP/OSi)$_2$
−30/−35	O=P(OP)$_n$(OSi$_{IV}$)$_m$
~−45	O=P(OSi$_{IV}$)$_n$(OSi$_{VI}$)$_m$
(^{29}Si)	
−90/−95	Si(OSi)$_2$(OH)$_2$ Q_2
~−100	Si(OSi)$_3$(OH) Q_3 or Si(OSi)(OH)$_2$(OP)
~−110	Si(OSi)$_4$ Q_4 or Si(OSi)$_2$(OP)(OH)
−110/−120	Si(OSi)$_{4-x}$(OP)$_x$ with $x = 1-3$

4. Conclusions

This paper has been devoted to the methodological characterization of the $\{^{31}P,^{29}Si\}$ spin pair by solid-state MAS NMR techniques. Experiments based on *J* and heteronuclear dipolar interaction were implemented using crystalline silicophosphate phases as model compounds. $Si_5O(PO_4)_6$ and various polymorphs of SiP_2O_7 were studied systematically by 2D $^{31}P \rightarrow {}^{29}Si$ CP MAS HETCOR, MAS-*J*-HMQC and MAS-*J*-INEPT experiments. The editing role of such experiments was clearly demonstrated. The $^{31}P-{}^{29}Si$ INEPT build-up curves allowed the measurement of $^2J_{P-O-Si}$ coupling constants. An unexpected dependence on both the coordination mode of the Si nuclei and the involved crystallographic paths has been demonstrated. Finally, $^{31}P \rightarrow {}^{29}Si$ CP MAS experiments were adapted to the characterization of Si−O−P mesoporous materials obtained by aerosol process. The results showing $^{31}P\cdots{}^{29}Si$ dipolar contacts are encouraging and will be compared in a near future to those obtained by MAS-*J*-derived techniques.

References

[1] (a) M.E. Davis, Nature 417 (2002) 813;
(b) A. Corma, Chem. Rev. 97 (1997) 2373;
(c) D. Brunel, Microporous Mesoporous Mater. 27 (1999) 329;
(d) J.Y. Ying, C.P. Mehnert, M.S. Wong, Angew Chem., Int. Ed. 38 (1999) 56.

[2] (a) M. Vallet-Regi, A. Ramila, R.P. del Real, J. Perez-Pariente, Chem. Mater. 13 (2001) 308;
(b) M. Vallet-Regi, L. Ruiz-Gonzalez, I. Izquierdo-Barba, J.M. Gonzalez-Calbert, J. Mater. Chem. 16 (2006) 26;
(c) B. Munoz, A. Ramila, J. Perez-Pariente, I. Diaz, M. Vallet-Regi, Chem. Mater. 15 (2003) 500.

[3] (a) J. Andersson, J. Rosenholm, S. Areva, M. Linden, Chem. Mater. 16 (2004) 4160;
(b) C. Charnay, S. Begu, C. Tourne-Peteilh, L. Nicole, D.A. Lerner, J.M. Devoisselle, Eur. J. Pharm. Biopharm. 57 (2004) 533;
(c) T. Azaïs, C. Tourne-Peteilh, F. Aussenac, N. Baccile, C. Coelho, J.-M. Devoisselle, F. Babonneau, Chem. Mater. 18 (2006) 6382.

[4] F. Balas, M. Manzano, P. Horcajada, M. Vallet-Regi, J. Am. Chem. Soc. 128 (2006) 8116.

[5] M. Vallet-Regi, I. Izquierdo-Barba, A. Ramila, J. Perez-Pariente, F. Babonneau, J.M. Gonzalez-Calbet, Solid State Sci. 7 (2005) 233.

[6] M.E. Neeraj, C.N.R. Rao, Mater. Res. Bull. 33 (1998) 1549.

[7] (a) S.R. Hartmann, E.L. Hahn, Phys. Rev. 128 (1962) 2042;
(b) A. Pines, G. Gibby, J.S. Waugh, J. Chem. Phys. 59 (1973) 569.

[8] D. Franke, R. Hudalla, R. Maxwell, H. Eckert, J. Phys. Chem. 96 (1992) 7506.

[9] (a) C. Coelho, T. Azaïs, L. Bonhomme-Coury, J. Maquet, C. Bonhomme, C. R. Chim. 9 (2006) 472;
(b) C. Lejeune, C. Coelho, L. Bonhomme-Coury, T. Azaïs, J. Maquet, C. Bonhomme, Solid State NMR 27 (2005) 242.

[10] (a) C.A. Fyfe, Y. Feng, H. Gies, H. Grondey, G.T. Kokotailo, J. Am. Chem. Soc. 112 (1990) 3264;
(b) C.A. Fyfe, K.C. Wong-Moon, Y. Huang, H. Grondey, J. Am. Chem. Soc. 117 (1995) 10397.

[11] D. Franke, C. Hudalla, H. Eckert, Solid State NMR 1 (1992) 33.

[12] (a) A. Lesage, D. Sakellariou, S. Steuernagel, L. Emsley, J. Am. Chem. Soc. 120 (1998) 13194;
(b) A. Lesage, P. Charmont, S. Steuernagel, L. Emsley, J. Am. Chem. Soc. 122 (2000) 9739.

[13] D. Massiot, F. Fayon, B. Alonso, J. Trebosc, J.-P. Amoureux, J. Magn. Reson. 164 (2003) 160.

[14] D. Iuga, C. Morais, Z. Gan, D.R. Neuville, L. Cormier, D. Massiot, J. Am. Chem. Soc. 127 (2005) 11540.

[15] C. Coelho, T. Azaïs, L. Bonhomme-Coury, J. Maquet, D. Massiot, C. Bonhomme, J. Magn. Reson. 179 (2006) 114.

[16] V. Montouillout, C.M. Morais, A. Douy, F. Fayon, D. Massiot, Magn. Reson. Chem. 44 (2006) 770.

[17] J.P. Amoureux, J. Trebosc, J. Wiench, M. Pruski, J. Magn. Reson. 184 (2007) 1.

[18] (a) G.A. Morris, R. Freeman, J. Am. Chem. Soc. 101 (1979) 760;
(b) D.P. Burum, R.R. Ernst, J. Magn. Reson. 39 (1980) 163;
(c) O.W. Sorensen, R.R. Ernst, J. Magn. Reson. 51 (1983) 477.

[19] (a) M.H. Levitt, Spin Dynamics, Basics of Nuclear Magnetic Resonance, Wiley, Chichester, 2002;
(b) J. Keeler, Understanding NMR Spectroscopy, Wiley, Chichester, 2005.

[20] (a) O. Soubias, V. Reat, O. Saurel, A. Milon, J. Magn. Reson. 158 (2002) 143;
(b) B. Alonso, D. Massiot, J. Magn. Reson. 163 (2003) 347.

[21] B. Elena, A. Lesage, S. Steuernagel, A. Böckmann, L. Emsley, J. Am. Chem. Soc. 127 (2005) 17296.

[22] (a) H.M. Kao, C.P. Grey, J. Magn. Reson. 133 (1998) 313.

[23] C.A. Fyfe, H. Meyer zu Altenschildesche, K.C. Wong-Moon, H. Grondey, J.M. Chezeau, Solid State NMR 9 (1997) 97.

[24] J.W. Wiench, M. Pruski, Solid State NMR 26 (2004) 51.

[25] H.M. Kao, C.P. Grey, J. Am. Chem. Soc. 119 (1997) 627.

[26] C. Coelho, T. Azaïs, L. Bonhomme-Coury, G. Laurent, C. Bonhomme, Inorg. Chem. 46 (2007) 1379.

[27] H. Mayer, Monatsh. Chem. 105 (1974) 46.

[28] H. Makart, Helv. Chim. Acta 50 (1967) 399.

[29] G. Bissert, F. Liebau, Acta Crystallogr. B26 (1970) 233.

[30] K.F. Hesse, Acta Crystallogr., Sect B 35 (1979) 724.
[31] (a) J. Brinker, Y. Lu, A. Sellinger, H. Fan, Adv. Mater. 11 (1999) 579;
(b) D. Grosso, G.J. de A.A. Soler-Illia, E.L. Crepaldi, B. Charleux, C. Sanchez, Adv. Funct. Mater. 13 (2003) 37;
(c) M.T. Bore, S.B. Rathod, T.L. Ward, A.K. Datye, Langmuir 19 (2003) 256;
(d) N. Baccile, D. Grosso, C. Sanchez, J. Mater. Chem. 13 (2003) 3011;
(e) N. Andersson, P.C.A. Alberius, J.S. Pedersen, L. Bergström, Microporous Mesoporous Mater. 72 (2004) 175.
[32] O.B. Peersen, X. Wu, I. Kustanovich, S.O. Smith, J. Magn. Reson. A 104 (1993) 334.
[33] D. Sakellariou, A. Lesage, L. Emsley, J. Magn. Reson. 151 (2001) 40.
[34] (a) D.T. Pegg, D.M. Doddrell, W.M. Brooks, M.R.J. Bendall, J. Magn. Reson. 44 (1981) 32;
(b) P. Lux, F. Brunet, H. Desvaux, J. Virlet, Magn. Reson. Chem. 31 (1993) 623.
[35] C. Coelho, F. Babonneau, T. Azaïs, L. Bonhomme-Coury, J. Maquet, G. Laurent, C. Bonhomme, J. Sol-Gel Sci. Technol. 40 (2006) 181.